Supplementary Information for robust frame-reduced structured illumination microscopy with accelerated correlation-enabled parameter estimation

Jiaming Qian[1,2,3,4], **Yu Cao**[1,2,3,4], **Kailong Xu**[1,2,3], **Ying Bi**[1,2,3], **Weiyi Xia**[1,2,3], **Qian Chen**[2], **and Chao Zuo**[1,2,3,*]

[1]Smart Computational Imaging (SCI) Laboratory, Nanjing University of Science and Technology, Nanjing,Jiangsu Province 210094, China.
[2]Smart Computational Imaging Research Institute (SCIRI) of Nanjing University of Science and Technology, Nanjing, Jiangsu Province 210019, China.
[3]Jiangsu Key Laboratory of Spectral Imaging & Intelligent Sense, Nanjing, Jiangsu Province 210094, China.
[*]zuochao@njust.edu.cn
[4]These authors contributed equally to this work.

ABSTRACT

This document provides supplementary information for "Robust frame-reduced structured illumination microscopy with accelerated correlation-enabled parameter estimation".

Contents

# Supplementary Note S1. Pixel-wise fluorescence pre-calibration

In order to solve the problem that the wide-field information in one direction can not be shared by others due to the fluorescence imbalance in the three illumination directions required for isotropic super-resolution, we propose a pixel-wise fluorescence pre-calibration approach. As can be seen in Fig. S1(a), for each illumination direction, traditional three-step phase-shifting illumination is used to solve the 0-order spectrums and the corresponding spatial wide-field image of an autofluorescent Ascaris lumbricoides sample with relatively uniform overall fluorescence distribution. Multi-frame averaging is used to remove ambient noise. For each wide-field image, we calculate the sum of the fluorescence intensities in a range of size 5×5 centered on each pixel. Then the ratio of the intensity sum of the first illumination direction to that of others in each pixel is obtained as the calibration parameter:

$$M_n(\mathbf{r}) = \frac{\sum\limits_{\mathbf{r}-2}^{\mathbf{r}+2} C_{n,0}(\mathbf{r})}{\sum\limits_{\mathbf{r}-2}^{\mathbf{r}+2} C_{1,0}(\mathbf{r})} \tag{S1}$$

where $n = 2$ and 3. Based on the calculated calibration parameters, the wide-field images of the second and third directions can be acquired directly from that of the first direction in the subsequent imaging:

$$C_{n,0}(\mathbf{r}) = M_n(\mathbf{r})C_{1,0}(\mathbf{r}) \tag{S2}$$

Figure S1(e) shows the wide-field images obtained by using the calculated calibration parameters [Fig. S1(b) and S1(c)] on the basis of $C_{1,0}$ [Fig. S1(d1) or S1(e1)], from which it can be seen that the wide-field information obtained by calibration is almost consistent with the actual version. In order to verify the availability and universality of the calibration parameters, we also performed the above calibration process for other regions of the Ascaris sample, and the calibration parameters obtained are almost identical to Fig. S1(b) and S1(c), with more than 90% of the parameters differing by less than 0.1 [Fig. S1(f)-S1(j)].
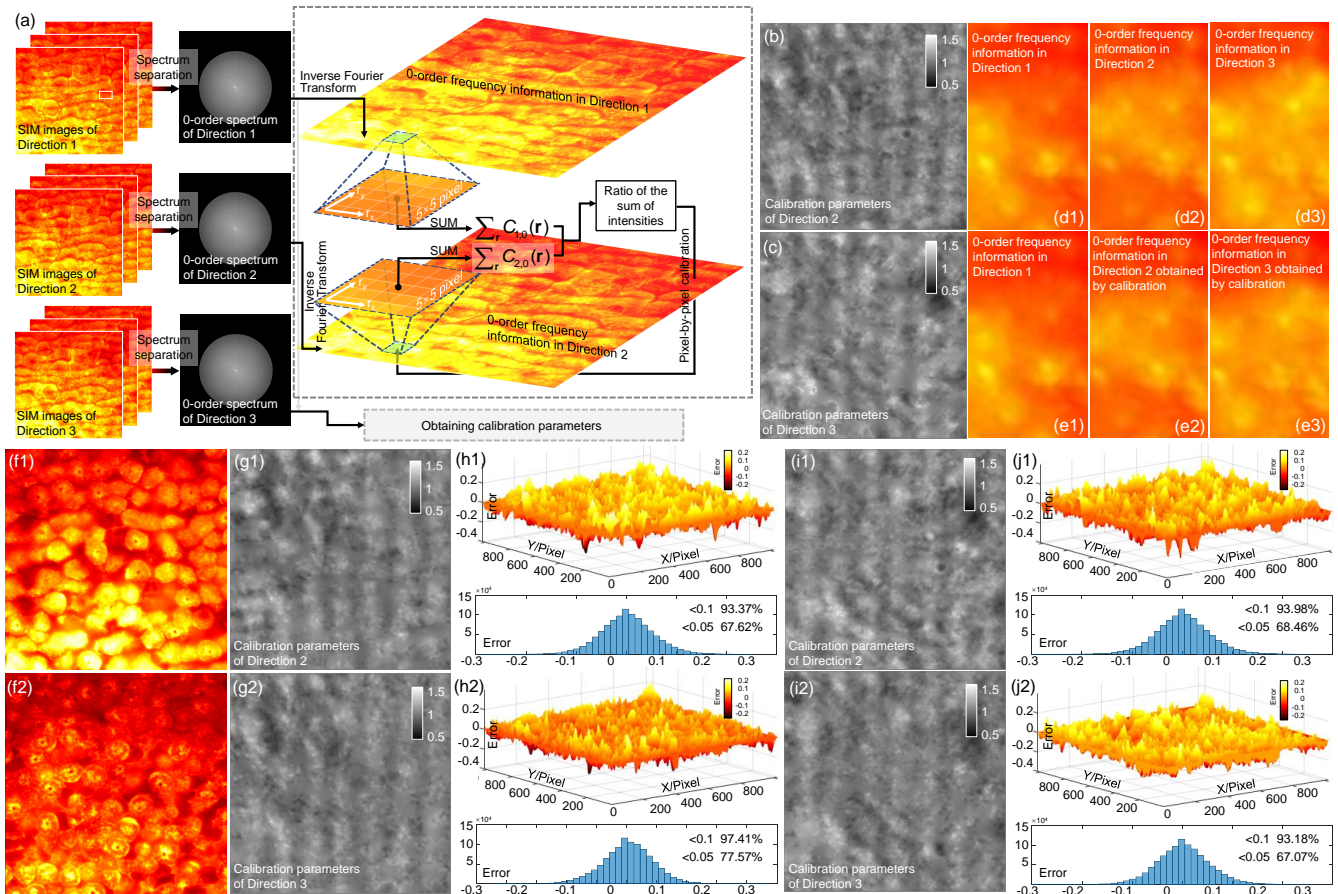
Figure S1. Flowchart of pixel-wise fluorescence pre-calibration and calibration results. (a) Flowchart of pixel-wise fluorescence pre-calibration taking a certain region of a Ascaris sample as an example. (b)-(c) Calibration parameters for the second and third illumination directions. (d) Magnified wide-field images from the white boxed region in (a) acquired from 3-step phase-shifting raw SIM images. (e) Magnified wide-field images from the white boxed regions in (a) acquired by calibration. (f) Wide-field images of the regions different from (a)-(e) in the first illumination direction. (g) Calibration parameters for the second illumination direction in regions of (f). (h) Error distribution and error histogram between (g) and (b). (i) Calibration parameters for the third illumination direction in regions of (f). (j) Error distribution and error histogram between (i) and (c).

Supplementary Note S2. Wiener filtering

After separating all the spectrum components from the 7 raw SIM images by accelerated correlation-enabled parameter estimation, Wiener filtering can be used to merge these spectrums in a weighted average manner:

$$\tilde{S}_{sim}(\mathbf{k}) = \frac{\sum_{n,j} \tilde{H}^*(\mathbf{k}+j\mathbf{p}_{n,j})\tilde{H}(\mathbf{k}+j\mathbf{p}_{n,j})\tilde{S}_{n,j}(\mathbf{k}+j\mathbf{p}_{n,j})}{\sum_{n,j}\left|\tilde{H}(\mathbf{k}+j\mathbf{p}_{n,j})\right|^2 + \omega^2} \tag{S3}$$

where ω is the Wiener constant (usually determined empirically). The final super-resolution image can be obtained by inverse Fourier transform:

$$I_{sim} = ifft(\tilde{S}_{sim}\tilde{A}) \tag{S4}$$

where $ifft$ represents the inverse Fourier transform and $\tilde{A}$ is a apodization function to suppress high-frequency artifacts (usually triangle, cosine or Gaussian function)[1–3].

Supplementary Note S3. Modulation-assigned spatial filter

We propose a modulation-assigned spatial filter to remove out-of-focus background due to thick sample scattering. In optical sectioning technique based on structured illumination, the modulation information is considered to be sharp only in the focus plane[4]. Similar conclusions also hold for the field of structured illumination three-dimensional imaging[5]. Based on such characteristics, it can be considered to remove unreliable backgrounds associated with low SNRs in advance according to the modulation distribution to avoid affecting the subsequent spectrum separation. Note that the modulation here, different from the modulation depth (a constant) of the illumination pattern in Eq. 1 of the main text, is a two-dimensional distribution associated with the degree of focus, which can be obtained by:

$$B = \frac{2}{3}\sqrt{[\sum_{j=1}^{3} D_{1,j}\sin\frac{2\pi(j-1)}{3}]^2 + [\sum_{j=1}^{3} D_{1,j}\cos\frac{2\pi(j-1)}{3}]^2} \tag{S5}$$

Figure S2a shows the wide-field image and the modulation image of actin in COS-7 cells (Fig. 5 in the main text), from which it can be seen that the modulation image has better sectioning capability. The histogram distributions of these images are shown in Fig. S2(b) and S2(c), respectively. For the wide-field histogram, the left peak represents the intensity of the dominant background, and the symmetric left-right distribution indicates fluctuations caused by ambient noise. There is also a second peak on the right side of Fig. S2(b) (dashed box), which is caused by defocusing, mixed with the sample information in both the spatial and frequency domains. Although the use of notch filter can suppress the defocus background, it will also change the spectrum information of the sample itself[6,7]. In the modulation histogram, the components of the main background increase significantly (the area with red solid lines) and there is no obvious additional peak in other regions, indicating that the sample information and the background have been spatially separated. We use twice the peak of the modulation histogram, the right boundary value of the solid red line, as the threshold to distinguish between background and sample information, and directly remove the regions with modulation less than the threshold. Although some sample information close to the right boundary of the background is also removed, these are signals with low SNRs prone to artifacts after being reconstructed. For extremely complex cases, where there are multiple peaks in the modulation histogram, we suggest dividing the original modulation image into multiple regions, and then solving the threshold of each sub region according to the above scheme.
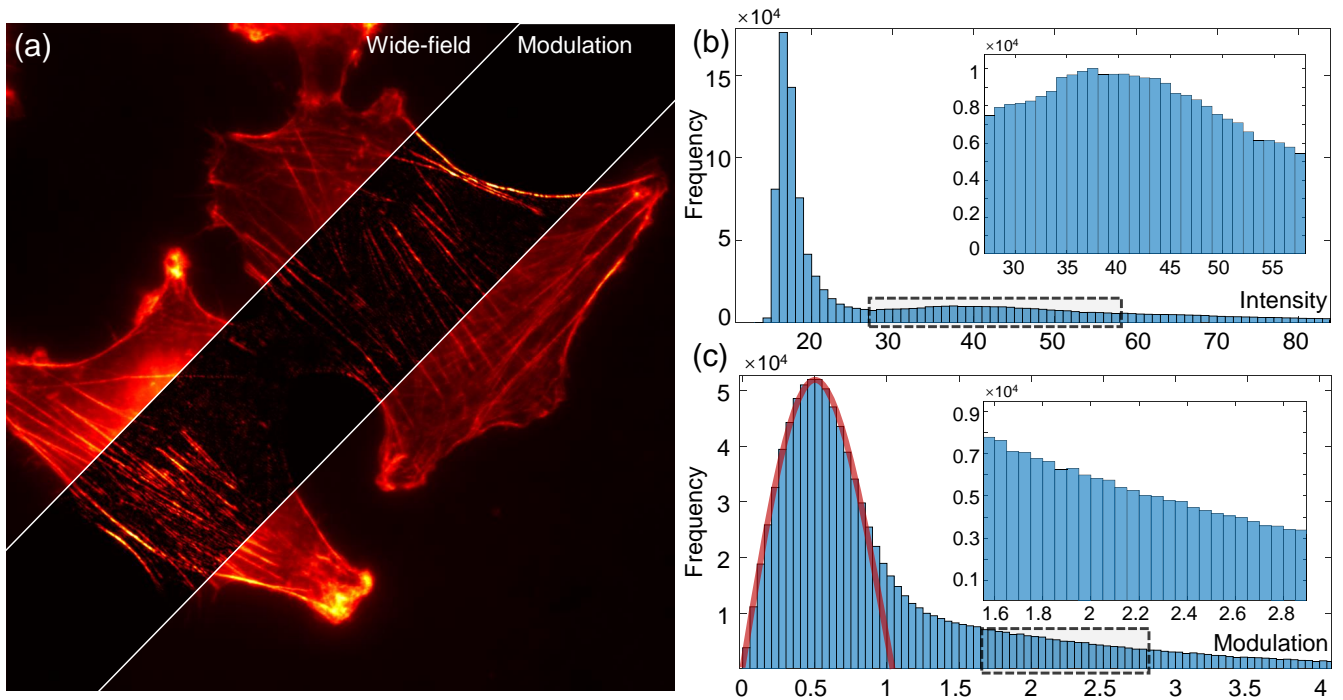
Figure S2. Wide-field image, modulation image and corresponding histograms of actin in a COS-7 cell sample. (a) Wide-field and modulation images of actin in a COS-7 cell sample. (b) Intensity histogram of the wide-field image. (c) Modulation histogram of the modulation image, where the red parabola indicates the area of the out-of-focus background.

Supplementary Note S4. SIM setup

Our SIM system is based on a commercial inverted fluorescence microscope (IX73, Olympus, Japan), including the microscope body and illuminated light path. The three lasers (OBIS405, OBIS561, Sapphire488, Coherent, USA) are coupled into a spatial filter through plane mirrors and dichroic mirrors, and transmitted through half-wave plates and polarization beam splitter. The structured light is generated by a ferroelectric-liquid-crystal spatial light modulator (FLC-SLM, QXGA-3DM, Fourth Dimension Displays, UK), and then the selected ±1-order diffracted beams by a specially designed mask pass through a 4f system and enter the IX73 microscope. The fine fringes are produced by the interference of two beams collected by the Oil immersion objective (UPlanXApo 60x/1.42 Oil, Olympus, Japan), and the period and direction of the pattern could be adjusted by SLM. Finally, a sCMOS camera (PCO Edge 5.5, PCO, Germany) was used to capture emission fluorescence images.

References

1. Gustafsson, M. G. *et al.* Three-dimensional resolution doubling in wide-field fluorescence microscopy by structured illumination. *Biophys. journal* **94**, 4957–4970 (2008).

2. Müller, M., Mönkemöller, V., Hennig, S., Hübner, W. & Huser, T. Open-source image reconstruction of super-resolution structured illumination microscopy data in imagej. *Nat. communications* **7**, 1–6 (2016).

3. Huang, X. *et al.* Fast, long-term, super-resolution imaging with hessian structured illumination microscopy. *Nat. biotechnology* **36**, 451–459 (2018).

4. Saxena, M., Eluru, G. & Gorthi, S. S. Structured illumination microscopy. *Adv. Opt. Photonics* **7**, 241–275 (2015).

5. Zuo, C., Huang, L., Zhang, M., Chen, Q. & Asundi, A. Temporal phase unwrapping algorithms for fringe projection profilometry: A comparative review. *Opt. lasers engineering* **85**, 84–103 (2016).

6. Wen, G. *et al.* High-fidelity structured illumination microscopy by point-spread-function engineering. *Light. Sci. & Appl.* **10**, 1–12 (2021).

7. Wang, Z. *et al.* High-speed image reconstruction for optically sectioned, super-resolution structured illumination microscopy. *Adv. Photonics* **4**, 026003 (2022).